Journal of Applied Physics

Reflectivity of solid and hollow microsphere composites and the effects of uniform and varying diameters

Cite as: J. Appl. Phys. **128**, 053103 (2020); https://doi.org/10.1063/5.0015650
Submitted: 05 June 2020 . Accepted: 13 July 2020 . Published Online: 04 August 2020

Ziqi Yu, Xiao Nie, Anil Yuksel, and Jaeho Lee

Journal of Applied Physics ARTICLE scitation.org/journal/jap

Reflectivity of solid and hollow microsphere composites and the effects of uniform and varying diameters

Cite as: J. Appl. Phys. **128**, 053103 (2020); doi: 10.1063/5.0015650
Submitted: 5 June 2020 · Accepted: 13 July 2020 ·
Published Online: 4 August 2020

Ziqi Yu,[1] Xiao Nie,[1] Anil Yuksel,[2] and Jaeho Lee[1,a)]

AFFILIATIONS

[1]Department of Mechanical and Aerospace Engineering, University of California, Irvine, California 92697, USA
[2]IBM Corporation, Austin, Texas 78758, USA

[a)]**Author to whom correspondence should be addressed:** jaeholee@uci.edu

ABSTRACT

While solid and hollow microsphere composites have received significant attention as solar reflectors or selective emitters, the driving mechanisms for their optical properties remain relatively unclear. Here, we study the solar reflectivity in the 0.4–2.4 μm wavelength range of solid and hollow microspheres with the diameter varying from 0.125 μm to 8 μm. SiO_2 and TiO_2 are considered as low- and high-refractive-index microsphere materials, respectively, and polydimethylsiloxane is considered as a polymer matrix. Based on the Mie theory and finite-difference time-domain simulations, our analysis shows that hollow microspheres with a thinner shell are more effective in scattering the light, compared to solid microspheres, and lead to a higher solar reflectivity. The high scattering efficiency, owing to the refractive-index contrast and large interface density, in hollow microspheres allows low-refractive-index materials to have a high solar reflectivity. When the diameter is uniform, 0.75 μm SiO_2 hollow microspheres provide the largest solar reflectivity of 0.81. When the diameter is varying, the randomly distributed 0.5–1 μm SiO_2 hollow microspheres provide the largest solar reflectivity of 0.84. The effect of varying diameter is characterized by strong backscattering in the electric field. These findings will guide optimal designs of microsphere composites and hierarchical materials for optical and thermal management systems.

INTRODUCTION

Passive radiative cooling using an outer space as the heat sink has revolutionized the thermal management of the building,[1,2] human body,[3,4] and deep space applications.[5] Among these materials,[1,3,6–12] particle–polymer composites are promising due to simple and scalable processing.[11,13] Numerous studies have shown effective radiative cooling using polymers with dielectric particle embedment with/without metal reflectors.[11,14,15] Alternative designs incorporating hollow particles achieve higher solar reflectivity due to the increased interface density.[16] Additionally, such a core–shell structure enables tunable material properties. Successful demonstrations of colored pigments,[17–19] spectrally selective photonic film,[20] climate-control building coatings,[21,22] thermal insulation,[23–25] and superhydrophobicity[19] have been realized. Recently, structural hierarchy, which already exists in nature,[26] has been employed as an additional knob to configure the optical properties of artificial materials. The size-dependent optical response of hierarchical building blocks provides broadband high reflectivity or absorptivity in the solar spectrum, thereby enabling far-reaching applications in novel radiative cooling films,[2] solar energy harvesting,[27] structural coloration,[28,29] and photocatalysis.[30] A noteworthy hierarchical cooling film developed by Peoples *et al.* lately demonstrated broadband-enhanced solar reflectivity by tuning the size composition of low-concentration TiO_2 nanoparticles of 104 ± 37 nm.[31] The efficacy of size hierarchy was supported by Monte Carlo and Mie theory calculations assuming individual scattering.[12,13] The composite with the optimized particle size constitution yields reflectivity higher than that of each building block, yet precise control on the particle size could be practically challenging. While hollow particles and structural hierarchy have individually demonstrated their effectiveness in achieving high solar reflectivity, their combined effect, to our best knowledge, has only received limited attention.[32] Our recent work demonstrated radiative cooling enabled by hollow glass microspheres with varying diameters but the effect of diameter variation

was not studied in detail.[33] In this letter, we performed systematic investigation on randomly closed-packed hollow SiO_2 microspheres in poly(dimethylsiloxane) (PDMS) with uniform and varying diameters ranging in 0.125–8 μm using the Mie theory and finite-difference time-domain (FDTD) calculations. By conducting single-particle Mie theory calculation, we identify geometric parameters that drive high reflectivity in wavelengths of 0.4–2.4 μm. By performing 2D FDTD simulations, which are valid and more computationally affordable[34] than previous approaches,[35–40] we investigate the effect of the shell thickness and material. Finally, the effect of diameter variation is studied, providing the guidance for future optimal designs of radiative cooling composites.

RESULTS AND DISCUSSION

We first compute the scattering efficiency $\boldsymbol{Q_{scat}}$ of single hollow microspheres in PDMS based on the Mie theory (see the supplementary material). We choose the outer diameter $\boldsymbol{d_o}$ of hollow microspheres varying from 0.5 to 8 μm. For each $\boldsymbol{d_o}$, we let the diameter, $\boldsymbol{d_i}$, of the air core, to increase from 0 to $\boldsymbol{d_o}$, where $\boldsymbol{d_i}$ of 0 and $\boldsymbol{d_o}$ are solid microspheres and porous PDMS, respectively. In Fig. 1(a), we plot $\boldsymbol{Q_{scat}}$ as colormaps to visualize its dependences

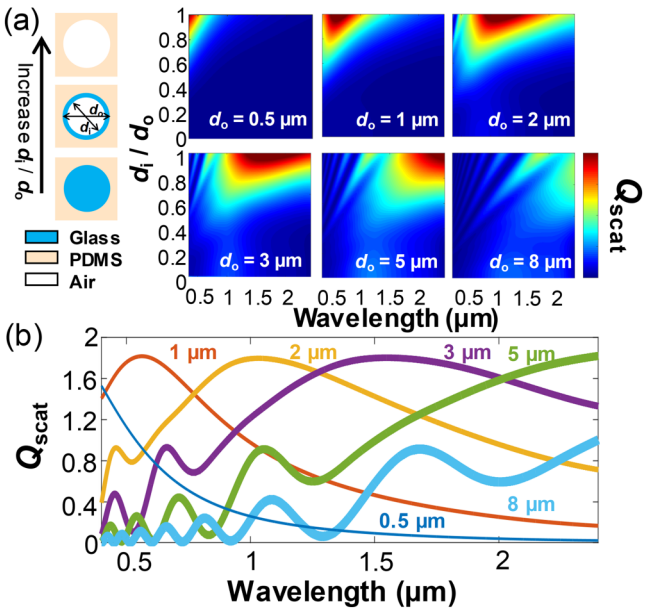

FIG. 1. (a) The scattering efficiency ($\boldsymbol{Q_{scat}}$) calculated using the Mie theory for individual hollow SiO_2 microspheres in a PDMS background in the wavelength range of 0.4–2.4 μm. The outer diameters $\boldsymbol{d_o}$ are varied from 0.5 to 8 μm, over which the scattering efficiency peaks redshift over the wavelength of interest. The shell thickness is indicated by the diameter ratio $\boldsymbol{d_i/d_o}$, which corresponds to the diameter of air core and SiO_2 microspheres, respectively. By changing from solid SiO_2 microspheres to porous PDMS, the scattering efficiency increases. (b) $\boldsymbol{Q_{scat}}$ as a function of wavelength for $\boldsymbol{d_i/d_o} = 0.9$. The diameter $\boldsymbol{d_o}$ is color-labeled correspondingly. The scattering efficiency shows peaks with locations and widths corresponding to $\boldsymbol{d_o}$. For $\boldsymbol{d_o} = 0.5$ and 8 μm, the scattering efficiency does not show the peak in the wavelength from 0.4 to 2.4 μm.

on $\boldsymbol{d_i/d_o}$ and the wavelength ($\boldsymbol{\lambda}$) (0.4–2.4 μm). We can make two key observations. First, by increasing the volume of the air, or decreasing shell thickness $\boldsymbol{t} = (\boldsymbol{d_o}-\boldsymbol{d_i})/2$, a hotspot representing high scattering efficiency appears for all $\boldsymbol{d_o}$ simulated. Second, the location of the high $\boldsymbol{Q_{scat}}$ on the spectrum redshifts as we increase $\boldsymbol{d_o}$. These results show the advantage of employing hollow structures that have a larger interface density. We define the interface density as $\varrho_{\text{int}} = \frac{\sum_N 4\pi r_N^2}{\frac{4}{3}\pi \max_N(r_N^3)}$, where $\boldsymbol{r}$ is the radius associated with each interface and $\boldsymbol{N}$ is the number of interfaces. Thus, for instance, a hollow microsphere with $\boldsymbol{d_i/d_o} = 0.9$ and $\boldsymbol{d_o} = 1$ μm has an interface density of 10.86 μm^{-1} and a solid microsphere with $\boldsymbol{d_o} = 1$ μm has an interface density of 6 μm^{-1}. Due to light scattering at the interface with refractive-index contrast, the hollow microspheres with greater interface densities lead to higher scattering efficiency and hence higher solar reflectivity. In Fig. 1(b), we set $\boldsymbol{d_i/d_o}$ to be 0.9 and plot the wavelength-dependent $\boldsymbol{Q_{scat}}$ curves. We can more clearly visualize the redshift of the $\boldsymbol{Q_{scat}}$ peak for $\boldsymbol{d_o}$ chosen. By increasing $\boldsymbol{d_o}$ from 1 μm to 5 μm, the peak of $\boldsymbol{Q_{scat}}$ shifts from approximately 0.5 to 2.4 μm on the spectrum; further increasing or decreasing $\boldsymbol{d_o}$ to 8 or 0.5 μm shift the peaks out of $\boldsymbol{\lambda} = 0.4$ to 2.4 μm.

We compute the spectral-average solar reflectivity $\langle R\rangle_\lambda = \frac{\int R(\lambda)d\lambda}{\int d\lambda}$ to compare composites with varying geometrical parameters. 2D FDTD simulations are performed in a $20 \times 100\,\mu m^2$ unit cell [Fig. S3(c)] periodically repeated in $\boldsymbol{x}$ with perfectly matched layers (PMLs) in $\boldsymbol{y}$. Using wider unit cells or finer mesh change results insignificantly (see Fig. S1), as the shell thickness and number of interfaces remain the same for 2D and 3D simulations. Our 2D model can capture the light transport and field information in the x–y plane, which is a cross section of the 3D hollow microsphere. Similar treatment using 2D FDTD models have been employed for 3D nanostructures including retinas,[1] nanodots,[2] and nanoparticles.[3] We illuminate the unit cell with a broadband (0.4–2.4 μm) unpolarized plane wave from below. Hollow microspheres are randomly generated in the unit cell[41] at the filling fraction (ff) of 55 vol. % [see Fig. S3(c)], which approaches the packing density of typical self-assembly structures.[29,42] The refractive indices of PDMS, SiO_2, and TiO_2 are from previous work.[43,44] To investigate the effect of shell thickness, we fix $\boldsymbol{d_o}$ of hollow SiO_2 microspheres to 1 μm. In Fig. 2(a), $\langle \boldsymbol{R}\rangle_\lambda$ increases from 0.04 to 0.77 by changing $\boldsymbol{d_i/d_o}$ from 0 to 1. When $\boldsymbol{d_i/d_o} = 0.9$, $\langle \boldsymbol{R}\rangle_\lambda$ peaks at 0.77, which outperforms those of solid microspheres and the porous PDMS. This could imply a significant reduction of coating thickness offered using hollow microsphere structures. From the point of view of refractive-index-contrast,[45] $\langle \boldsymbol{R}\rangle_\lambda$ depends strongly on the air (n_{glass}–n_{air} is the largest contrast in this system) core size, $\boldsymbol{d_i}$, where larger $\boldsymbol{d_i}$ offers greater interface-to-volume ratio and thus enhanced scattering efficiency. The propagation of light is randomized due to repeated scattering by the air core which shortens photon transport mean free path[46] and hence strengthens reflection. To compare, we replace SiO_2 with TiO_2. The increased refractive-index-contrast lifts $\langle \boldsymbol{R}\rangle_\lambda$ significantly, ranging from 0.84 to 0.93 when varying $\boldsymbol{d_i/d_o}$ from 0 to 0.9. $\langle \boldsymbol{R}\rangle_\lambda$ of 0.93 at $\boldsymbol{d_i/d_o} = 0.7$ is not only a 20.5% enhancement than that of hollow SiO_2 microspheres with $\boldsymbol{d_i/d_o} = 0.9$ but also a 21.5% increment than the porous PDMS. We attribute the increased $\langle \boldsymbol{R}\rangle_\lambda$ to the additional light scattering induced by high-refractive-index shells. As shown in the inset, the

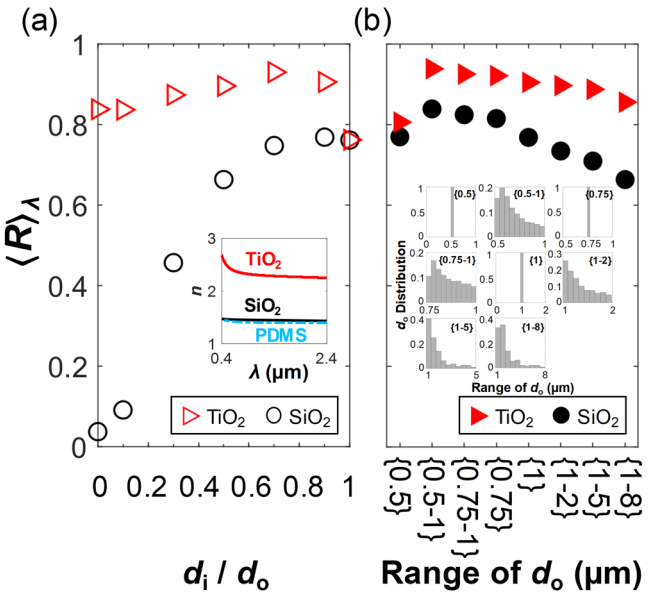

FIG. 2. (a) Integrated reflectivity $\langle R \rangle_\lambda$ as a function of shell thickness for uniform-diameter hollow SiO_2 and TiO_2 microspheres with $d_o = 1\,\mu m$ in the wavelength range of 0.4–2.4 μm. (b) $\langle R \rangle_\lambda$ of varying-diameter hollow SiO_2 microspheres with d_o ranges in {0.5–1}, {0.75–1}, {1–2}, {1–5}, and {1–8} μm. $\langle R \rangle_\lambda$ computed for the uniform-diameter microspheres, {0.5}, {0.75}, and {1} μm, are plotted for comparison. The shell thickness defined by $d_i/d_o = 0.9$ is studied.

refractive index of TiO_2 varies from approximately 2.6 to 2.2 between the wavelength of 0.4 and 2.4 μm, whereas the refractive indices of SiO_2 and PDMS are very close to each other and almost maintain invariant in the same wavelength range. The refractive-index contrast between SiO_2 and PDMS varies from 0.006 to 0.048, whereas that between TiO_2 and PDMS varies from 0.855 to 1.216 in the wavelength range of 0.4 to 2.4 μm. Interestingly, $\langle R \rangle_\lambda$ of hollow SiO_2 microspheres with $d_i/d_o = 0.9$ is only an 8.3% reduction from $\langle R \rangle_\lambda$ of solid TiO_2 microspheres, making the former a promising low-refractive-index alternative for the latter considering its strong ultraviolet (UV) absorption and potential safety concerns.[14] Moving on to the effect of diameter variation, we find that $\langle R \rangle_\lambda$ increases with increasing d_i/d_o even though d_o is not uniform (see Fig. S2 in the supplementary material). In Fig. 2(b), for $d_i/d_o = 0.9$, $\langle R \rangle_\lambda$ generally decreases as the diameter variation extends toward larger d_o and increases as the variation expands to the nanoscale. Notably, $\langle R \rangle_\lambda$ drops by 8.3% from 0.84 to 0.77 as d_o varies from {0.5–1} to 0.5 μm; further increasing d_o to {0.75–1} and 0.75 μm leads to slight reflectivity reductions (to 0.825 and 0.815, respectively), while still maintaining the advantage of the varying-over uniform-diameter design. Hollow SiO_2 microspheres with the varying d_o induce scattering efficiency peaks located differently over the entire solar spectrum [Fig. 1(b)]; scattering efficiency dips associated with certain sizes are successfully compensated by others (see Fig. S3). The diameter variation thus provides broadband solar reflectivity enhancement in the hollow SiO_2 microsphere composites. We notice that the varying-diameter hollow microspheres with submicrometer sizes made of both SiO_2 and TiO_2 show similar reflectivities. This could be due to the fact that the structure factor of the disordered structures has similar Fourier transforms in the short k range, thus yield similar scattering properties. Note that the distribution of d_o is skewed toward smaller sizes [inset of Fig. 2(b)], however, at the filling ratio of 55 vol. %, we do not observe significant effect on the solar reflectivity from varying the current size distribution to a normal one (see Fig. S4).

To explain the trend of $\langle R \rangle_\lambda$ in Fig. 2(b), we employ the total-field scattered-field (TFSF) source to illuminate randomly distributed hollow SiO_2 microspheres with varying d_o in a $20 \times 20\,\mu m^2$ unit cell (ff = 55 vol. %) surrounded by PMLs. Statistics of d_o distribution (bottom left inset) are close to those in Fig. 2(b). We compute the backscattering ratio Q_b/Q_f, where Q_b and Q_f are the scattering efficiency in the forward and backward directions, respectively, defined by angular ranges [0, 180°) and [180°, 360°) from the $+x$ direction (schematics in Fig. 3). We selectively consider varying d_o distributions of 0.5 to 1 μm, 1 to 2 μm, 1 to 5 μm, and 1 to 8 μm, which for brevity will be referred to as {0.5–1}, {1–2}, {1–5}, and {1–8}, respectively, hereafter. Uniform-diameter hollow SiO_2 microspheres with d_o of 0.5 and 1 μm (referred to as {0.5 and {1}) are included for comparison. The backscattering ratio of the composites {1–2}, {1–5}, and {1–8} with $d_i/d_o = 0.9$ shares a similar decreasing trend, while differing in magnitudes over the entire spectrum. Composites {0.5}, {0.5–1}, and {1} yield comparable backscattering ratio in the visible spectrum, while in the near-IR range show similar major peaks/dips but contrasting amplitudes. Specifically, varying d_o distribution compensates the dip at $\lambda \approx 1.2\,\mu m$ and lowers the peak near $\lambda \approx 1.8\,\mu m$. Notably, composites with smaller d_o achieve spectral-average backscattering ratio $\langle Q_b/Q_f \rangle_\lambda$ (bottom right inset), which could be due to stronger scattering by increased number of scatterers as d_o decreases. Importantly, despite higher backscattering ratio from around 1 to 1.6 μm for the composite {0.5} than {0.5–1}, the former exhibits a significant reduction after 1.6 μm, resulting in higher $\langle Q_b/Q_f \rangle_\lambda$ which agrees well with the trend in Fig. 2(b). We also selectively plot the electric field distribution for composites {0.5–1} and {1} at the backscattering ratio peaks and dips to reveal the optical behavior underlying the enhanced reflection. At $\lambda = 1.81$ and 1.84 μm, greater electric field magnitude $|E|$ in the backward direction indicates stronger backscattering, whereas at $\lambda = 1.47$ and 2.33 μm, $|E|$ is larger in the forward direction which indicates stronger forward scattering. SiO_2 microspheres with thicker shells exhibit strikingly different scattering properties (see Fig. S5 in the supplementary material for details).

$\langle R \rangle_\lambda$ and $\langle Q_b/Q_f \rangle_\lambda$ concurrently imply stronger solar reflection achieved by hollow SiO_2 microspheres with nanoscale d_o. To reduce computational cost, we compute $\langle Q_b/Q_f \rangle_\lambda$ for hollow SiO_2 microspheres with varying and uniform diameter in a submicrometer scale while keeping $d_i/d_o = 0.9$. Depicted in Fig. 4(a), $\langle Q_b/Q_f \rangle_\lambda$ for uniform-diameter hollow SiO_2 microspheres' peaks at 0.5 μm and quickly decays toward both ends. Similarly, for varying-diameter hollow SiO_2 microspheres in (b), $\langle Q_b/Q_f \rangle_\lambda$ reaches comparable apexes for d_o ranging in {0.25–1} and {0.5–1} μm, whereas extending the range further toward smaller and larger sizes yields reduced backscattering. Specifically, shown in the inset, the two optimal varying-diameter designs slightly outperform the uniform-

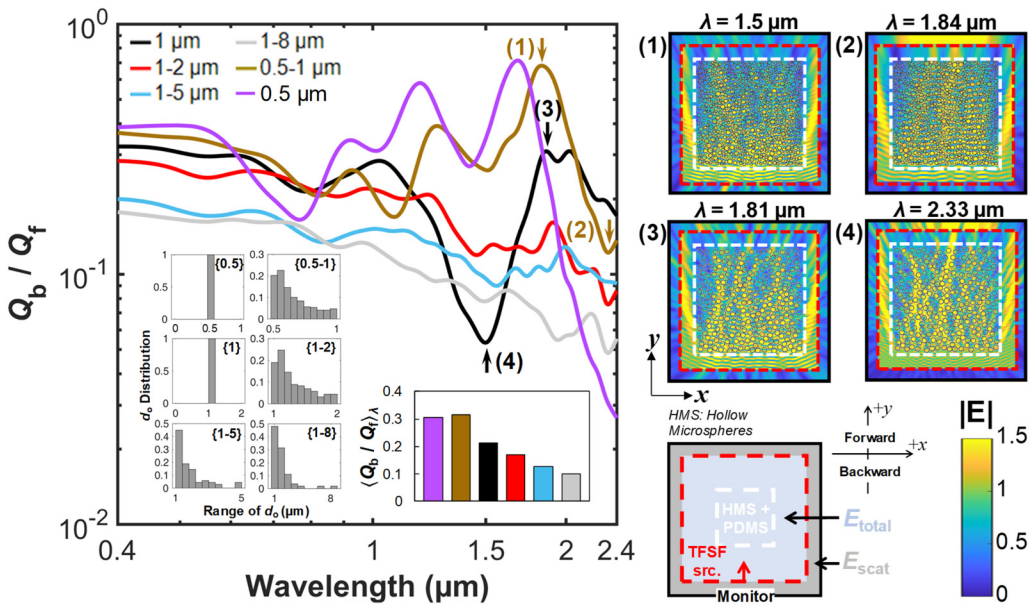

FIG. 3. Wavelength-dependent backscattering ratio computed for varying-diameter hollow SiO_2 microspheres with d_i/d_o. The simulation is performed using $20 \times 20\,\mu m^2$ unit cells illuminated by the total-field scattered-field source in the wavelength range of 0.4–2.4 μm. The statistical distribution of d_o is similar to that in Fig. 2(b). Selected electric fields of uniform- ($d_o = 1\,\mu m$) and varying-diameter ($d_o = 0.5$ to 1 μm) hollow SiO_2 microspheres with $d_i/d_o = 0.9$. In the field images, the boundary of hollow microspheres is depicted as white-dashed boxes; the boundary of the TFSF source is depicted as red-dashed boxes; the monitor is depicted as black solid boxes. A schematic to show the placements of hollow microspheres, TFSF source, and monitor is presented below the field images. And, the color scale is presented on its right.

diameter design ($d_o = 0.5\,\mu m$) in $\langle Q_b/Q_f \rangle_\lambda$, which highlights the advantage of diameter variation. Yet, we notice that in Fig. 2(b), composite {0.5} has the lowest $\langle R \rangle_\lambda$, differing from $\langle Q_b/Q_f \rangle_\lambda$. We could attribute this to the difference in the simulated unit cells,

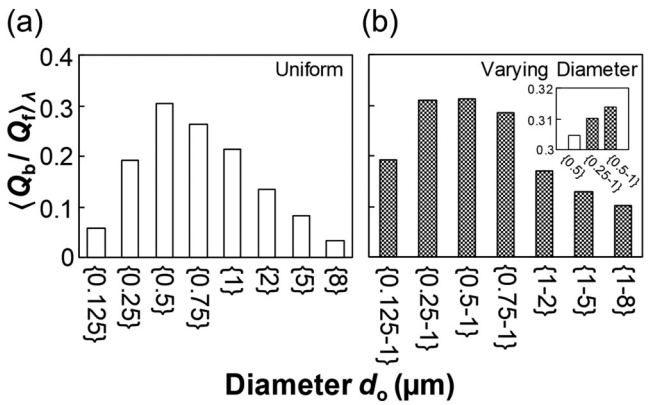

FIG. 4. Spectral-average backscattering ratio $\langle Q_b/Q_f \rangle_\lambda$ of (a) uniform- and (b) varying-diameter hollow SiO_2 microspheres with $d_i/d_o = 0.9$. Uniform-size hollow SiO_2 microspheres induce the highest backscattering ratio when $d_o = 0.5\,\mu m$; hollow SiO_2 microspheres with varying d_o ranging in {0.25–1} and {0.5–1} μm provide comparably high backscattering ratios, which slightly outperform that of uniform-size ({0.5} μm). The inset plots $\langle Q_b/Q_f \rangle_\lambda$ for hollow SiO_2 microspheres with d_o of {0.5}, {0.25–1}, and {0.5–1} μm, respectively.

whereas the advantage of varying-diameter over the uniform-diameter design in offering high $\langle R \rangle_\lambda$ maintains and trends of $\langle R \rangle_\lambda$ and $\langle Q_b/Q_f \rangle_\lambda$ for other diameters agree well. When d_o is uniform, the reduced $\langle Q_b/Q_f \rangle_\lambda$ could be due to narrowband scattering efficiency peaks at specific wavelengths, inferred by Fig. 1; when d_o is varying, scattering efficiency peaks inherited to multiple sizes blend to induce a broadband enhancement. The optimal $\langle Q_b/Q_f \rangle_\lambda$ in (b) implies a competing effect between the increased number of scatterers due to decreased d_o, which would lead to enhanced scattering, and the scattering efficiency, whose peak blueshifts with decreasing d_o. Importantly, we consider only the range of d_o but not specific combinations, which relaxes the stringent requirement of precise control on size compositions that may be practically challenging.

To discuss, we do not consider UV or mid-infrared (mid-IR) spectra as they only account for 11% of solar irradiation.[47] Additional insight into spectral contributions is obtained by computing $\langle R \rangle_\lambda$ in UV (7%), visible (44%), near-IR (45%), and mid-IR (4%) by their percentages in solar power (100%). For the optimal hollow SiO_2 microspheres with d_o of {0.5–1} μm, we assume that $\langle R \rangle_{\lambda,UV}$ and $\langle R \rangle_{\lambda,mid\text{-}IR}$ are 0 to 1 and yield $\langle R \rangle_{\lambda,vis} = 0.868$ and $\langle R \rangle_{\lambda,near\text{-}IR} = 0.821$, respectively, leading to a weighted $\langle R \rangle_\lambda$ from UV to mid-IR ranging from 0.751 to 0.861. For λ from 0.4 to 2.4 μm, higher $\langle R \rangle_\lambda$ is expected for composites thicker than 100 μm due to decreased transmissivity led by the addition of materials (see Fig. S6). By incorporating hollow microsphere structures with a thinner shell, a solar reflectivity that is significantly higher than that of solid microspheres of the same material can be achieved. A

solid microsphere composites will need a much thicker film to realize similar solar reflectivity.[15] Therefore, hollow microspheres can be significantly helpful as thin coating materials, such as for radiative cooling, with a lighter weight at the meanwhile due to the material removal. For λ smaller than 0.4 μm, we expect high UV reflectivity from hollow SiO_2 microspheres thanks to the sizes comparable with λ in varying diameter distributions, whereas TiO_2 microspheres would suffer from strong UV absorption. For wavelengths greater than 2.4 μm, $\langle R \rangle_\lambda$ for both SiO_2 or TiO_2 hollow microspheres would drop significantly due to increased absorptivity/emissivity. For radiative cooling, one also desires a low reflectivity in the atmospheric window ($\lambda = 8$–13 μm). In this regard, we simulated the 0.5–1 μm varying-diameter SiO_2 microspheres and the result (Fig. S7) shows a reflectivity always below 0.1, which is suitable for the radiative cooling application where a high emissivity is required to lose heat in this wavelength range. One could adjust the range of varying diameters to achieve solar reflectivity modulation according to the need. Generally, hollow microspheres with varying diameters defined by ranges without fine tuning specific size compositions discussed here will benefit applications where broadband optical responses are desired.

CONCLUSIONS

We have studied the solar reflectivity in the 0.4–2.4 μm wavelength range of solid and hollow microspheres with the diameter varying from 0.125 to 8 μm using the Mie theory and FDTD simulations. SiO_2 and TiO_2 are considered as low- and high-refractive-index microsphere materials, while the PDMS is considered as a polymer matrix. Our analysis has shown that hollow microspheres with a thinner shell are more effective in scattering light, compared to solid microspheres, and lead to a higher solar reflectivity up to 20 times. The high scattering efficiency, owing to the refractive-index contrast and large interface density, in hollow microspheres allows low-refractive-index materials to have a high solar reflectivity of 0.77, which is only 8.3% less than that of solid TiO_2 microspheres. When the diameter is uniform, 0.75 μm SiO_2 hollow microspheres provide the largest solar reflectivity of 0.81. When the diameter is varying, the random-distributed 0.5–1 μm SiO_2 hollow microspheres provide the largest solar reflectivity of 0.84. The effect of varying diameter is further supported by the backscattering ratio, where hollow SiO_2 microspheres with 0.5–1 μm diameters achieve the strongest backscattering among all studied designs. These findings will guide optimal designs of microsphere composites and hierarchical materials for optical and thermal management systems.

SUPPLEMENTARY MATERIAL

See the supplementary material for details of Mie theory calculation, a convergence test for FDTD simulations, and additional simulation results related to varying-diameter hollow SiO_2 microspheres with different shell thicknesses, spectral-dependent solar reflectivity corresponding to results presented in Fig. 2, the effect of varying distributions of hollow SiO_2 microspheres, and the effect of the hollow SiO_2 microspheres' composite thickness.

ACKNOWLEDGMENTS

Z.Y., X.N., and J.L. would like to acknowledge support by the Henry Samueli School of Engineering at UCI. Z.Y. and J.L. thank the support provided by the National Science Foundation (No. ECCS-1935843). X.N. thanks the support provided by the California Energy Commission (No. EPC-17-045).

DATA AVAILABILITY

The data that support the findings of this study are available from the corresponding author upon reasonable request.

REFERENCES

[1]T. Li, Y. Zhai, S. He, W. Gan, Z. Wei, M. Heidarinejad, D. Dalgo, R. Mi, X. Zhao, J. Song, J. Dai, C. Chen, A. Aili, A. Vellore, A. Martini, R. Yang, J. Srebric, X. Yin, and L. Hu, Science **364**, 760 (2019).
[2]J. Mandal, Y. Fu, A. C. Overvig, M. Jia, K. Sun, N. N. Shi, H. Zhou, X. Xiao, N. Yu, and Y. Yang, Science **362**, 315 (2018).
[3]P. C. Hsu, C. Liu, A. Y. Song, Z. Zhang, Y. Peng, J. Xie, K. Liu, C. L. Wu, P. B. Catrysse, L. Cai, S. Zhai, A. Majumdar, S. Fan, and Y. Cui, Sci. Adv. **3**, e1700895 (2017).
[4]P. C. Hsu, A. Y. Song, P. B. Catrysse, C. Liu, Y. Peng, J. Xie, S. Fan, and Y. Cui, Science **353**, 1019 (2016).
[5]R. C. Youngquist, M. A. Nurge, W. L. Johnson, T. L. Gibson, and J. M. Surma, J. Spacecr. Rockets **55**(3), 622 (2018).
[6]D. Xie, Z. Yang, X. Liu, S. Cui, H. Zhou, and T. Fan, Soft Matter **15**, 4294 (2019).
[7]L. Cai, A. Y. Song, P. Wu, P. C. Hsu, Y. Peng, J. Chen, C. Liu, P. B. Catrysse, Y. Liu, A. Yang, C. Zhou, C. Zhou, S. Fan, and Y. Cui, Nat. Commun. **8**, 496 (2017).
[8]B. Dai, K. Li, L. Shi, X. Wan, X. Liu, F. Zhang, L. Jiang, and S. Wang, Adv. Mater. **31**, 1904113 (2019).
[9]D. Fan, H. Sun, and Q. Li, Sol. Energy Mater. Sol. Cells **195**, 250 (2019).
[10]Y. Peng, J. Chen, A. Y. Song, P. B. Catrysse, P. C. Hsu, L. Cai, B. Liu, Y. Zhu, G. Zhou, D. S. Wu, H. R. Lee, S. Fan, and Y. Cui, Nat. Sustain. **1**, 105 (2018).
[11]Y. Zhai, Y. Ma, S. N. David, D. Zhao, R. Lou, G. Tan, R. Yang, and X. Yin, Science **355**, 1062 (2017).
[12]L. Zhou, H. Song, J. Liang, M. Singer, M. Zhou, E. Stegenburgs, N. Zhang, C. Xu, T. Ng, Z. Yu, B. Ooi, and Q. Gan, Nat. Sustain. **2**, 718 (2019).
[13]Z. Cheng, F. Wang, H. Wang, H. Liang, and L. Ma, Int. J. Therm. Sci. **140**, 358 (2019).
[14]Z. Huang and X. Ruan, Int. J. Heat Mass Transfer **104**, 890 (2017).
[15]S. Atiganyanun, J. B. Plumley, S. J. Han, K. Hsu, J. Cytrynbaum, T. L. Peng, S. M. Han, and S. E. Han, ACS Photonics **5**, 1181 (2018).
[16]Z. Xing, S. W. Tay, Y. H. Ng, and L. Hong, ACS Appl. Mater. Interfaces **9**(17), 15103 (2017).
[17]G. Zeng, J. Yang, R. Hong, Z. Li, Y. Chen, F. Li, Q. Wu, L. Liu, and X. Jiang, Ceram. Int. **44**(8), 8788 (2018).
[18]Q. Gao, X. Wu, D. Lu, and Y. Fan, Dyes Pigm. **154**, 21 (2018).
[19]Q. Gao, X. Wu, Y. Fan, and Q. Meng, Sol. Energy Mater. Sol. Cells **180**, 138 (2018).
[20]Y. Lim, S. Lee, Y. Li, S.-H. Kim, T. H. Kang, Y. D. Suh, S. Lee, Y. Kim, and G.-R. Yi, Part. Part. Syst. Charact. **37**, 1900405 (2020).
[21]M. Čekon, M. Kalousek, J. Hraška, and R. Ingeli, Energy Build. **77**, 343 (2014).
[22]O. Sandin, J. Nordin, and M. Jonsson, J. Coat. Technol. Res. **14**(4), 817 (2017).
[23]Q. Cai, H. Ye, and Q. Lin, Appl. Therm. Eng. **100**, 468 (2016).
[24]L. Gong, Y. Wang, X. Cheng, R. Zhang, and H. Zhang, Int. J. Heat Mass Transfer **67**, 253 (2013).
[25]G. Shang, P. Dyachenko, E. W. Leib, T. Vossmeyer, A. Petrov, and M. Eich, Ceram. Int. **46**(11PB), 19241 (2020).

[26]B. A. Palmer, V. J. Yallapragada, N. Schiffmann, E. M. Wormser, N. Elad, E. D. Aflalo, A. Sagi, S. Weiner, L. Addadi, and D. Oron, Nat. Nanotechnol. **15**, 138 (2020).
[27]M. Chen, J. Mandal, Q. Ye, A. Li, Q. Cheng, T. Gong, T. Jin, Y. He, N. Yu, and Y. Yang, ACS Appl. Energy Mater. **2**, 6551 (2019).
[28]N. Schneider, C. Zeiger, A. Kolew, M. Schneider, J. Leuthold, H. Hölscher, and M. Worgull, Opt. Mater. Express **4**, 1895 (2014).
[29]G. Shang, Y. Häntsch, K. P. Furlan, R. Janßen, G. A. Schneider, A. Petrov, and M. Eich, APL Photonics **4**(4), 046101 (2019).
[30]J. Zhuang, Q. Tian, H. Zhou, Q. Liu, P. Liu, and H. Zhong, J. Mater. Chem. **22**(14), 7036 (2012).
[31]J. Peoples, X. Li, Y. Lv, J. Qiu, Z. Huang, and X. Ruan, Int. J. Heat Mass Transfer **131**, 487 (2019).
[32]J. D. Alden, S. Atiganyanun, R. Vanderburg, S. H. Lee, J. B. Plumley, O. K. Abudayyeh, S. M. Han, and S. E. Han, J. Photonics Energy **9**(3), 032705 (2019).
[33]X. Nie, Y. Yoo, H. Hewakuruppu, J. Sullivan, A. Krishna, and J. Lee, Sci. Rep. **10**, 6661 (2020).
[34]G. Jacucci, J. Bertolotti, and S. Vignolini, Adv. Opt. Mater. **7**(23), 1900980 (2019).
[35]A. Yuksel, E. T. Yu, M. Cullinan, and J. Murthy, J. Photonics Energy **9**(3), 1 (2019).
[36]E. Tervo, M. Francoeur, B. Cola, and Z. Zhang, Phys. Rev. B **100**, 205422 (2019).
[37]A. Yuksel, E. Tervo, B. Cola, and J. Murthy, in *Proceedings of 16th Intersocial Conference on Thermal Thermomechanical Phenomenon in Electronic Systems ITherm 2017* (IEEE, 2017).
[38]S. S. Abdallah, O. Ramahi, and K. Bizheva, in *Annual International Conference on IEEE Engineering and. Medical Biology Proceedings* (IEEE, 2007).
[39]J. Y. Park, J. Ham, I. Lee, and J. L. Lee, Nanoscale **10**, 14868 (2018).
[40]Y. Chen, J. Wang, T. Xu, M. Liu, J. Liu, H. Huang, and F. Ouyang, Curr. Appl. Phys. **20**, 391 (2020).
[41]Y. Zhang, Y. Xu, S. Chen, H. Lu, K. Chen, Y. Cao, A. E. Miroshnichenko, M. Gu, and X. Li, ACS Appl. Mater. Interfaces **10**(19), 16776 (2018).
[42]D. L. Wood, K. Nassau, and D. L. Chadwick, Appl. Opt. **21**(23), 4276 (1982).
[43]E. D. Palik, *Handbook of Optical Constants of Solids* (Academic Press, 2012).
[44]M. Querry, Contract. Rep. Contract. Report CRDEC-CR-88009 pp. 1–331 (1987).
[45]P. D. García, R. Sapienza, Á Blanco, and C. López, Adv. Mater. **19**(18), 2597 (2007).
[46]M. Burresi, L. Cortese, L. Pattelli, M. Kolle, P. Vukusic, D. S. Wiersma, U. Steiner, and S. Vignolini, Sci. Rep. **4**, 6075 (2015).
[47]R. Youngquist, A. Krenn, T. Gibson, S. Snyder, W. Johnson, and J. Wendell, *Cryogenic Thermal Control Coatings: An Overview* (NASA, Cocoa Beach, FL, 2020).